Journal of Photochemistry & Photobiology, A: Chemistry 462 (2025) 116218

Contents lists available at ScienceDirect

Journal of Photochemistry & Photobiology, A: Chemistry

journal homepage: www.elsevier.com/locate/jphotochem

Novel cyclometalated iridium (III) complexes as antibacterial agents for photodynamic inactivation

Muireann Fallon [a,1,2], Ralte Lalrempuia [b,c,2], Leila Tabrizi [b], Michael P. Brandon [b], Ross McGarry [b], Aoibhín Cullen [b], Francisco J. Fernández-Alvarez [d], Mary T. Pryce [b,*], Deirdre Fitzgerald-Hughes [a,*]

[a] Department of Clinical Microbiology, Royal College of Surgeons in Ireland, Beaumont Hospital, Dublin 9, Ireland
[b] School of Chemical Sciences, Dublin City University, Dublin, Ireland
[c] Department of Chemistry, School of Physical Sciences, Mizoram University, Aizawl, Mizoram, India
[d] Departamento de Química Inorgánica-Instituto de Síntesis Química y Catálisis Homogénea (ISQCH), Universidad de Zaragoza–CSIC, Facultad de Ciencias, 50009 Zaragoza, Spain

ARTICLE INFO

Keywords:
Cyclometalated iridium(III) complex
Antimicrobial photodynamic therapy
Photosensitizer
Singlet oxygen
Photo-sterilisation
Transient spectroscopy
Electrochemistry

ABSTRACT

Staphylococcus aureus and methicillin-resistant *S. aureus* (MRSA) frequently cause chronic skin and soft tissue infections and device-related infections. These bacteria colonize human skin and can survive for long periods within biofilms, on indwelling medical devices, high touch surfaces and equipment in the healthcare setting, which are reservoirs for further transmission to patients. Photodynamic therapy may offer an alternative to antibiotics in the management of infections or photodynamic disinfection may limit transmission of specific pathogens in the healthcare setting. Two novel cyclometalated iridium (III) complexes $[Ir(ppy)_2L](PF_6)$ (ppy: phenyl pyridine, L = 6-((2,6-diisopropylphenyl)amino)-5,6-dihydro-1,10-phenanthrolin-5-ol (**Ir1**) and L = N-(2,6-diisopropylphenyl)-1,10-phenanthrolin-5-amine (**Ir2**)) were synthesized and evaluated for their antimicrobial properties when activated by light (370 nm). Iridium complexes (**Ir1** and **Ir2**) led to potent inactivation of planktonic *Staphylococcus aureus* at 5 μM (almost 5 $\log_{10}$ reduction in colony forming units (CFU)/mL) after light exposure ($p \leq 0.01$ for dark *vs* light). Dark toxicity was < 1 $\log_{10}$. Under the same conditions, *Escherichia coli* killing was < 1 $\log_{10}$. Anti-staphylococcal activity was concentration-dependant over the range 0.1 μM – 5 μM ($p \leq 0.001$, **Ir1**, $p \leq 0.01$ **Ir2**). Anti-biofilm activity was observed against mature (72 h) biofilms of *S. aureus* including methicillin-resistant *S. aureus* (MRSA) biofilms but higher concentrations (50 μM) were required. Treatment with **Ir1** or **Ir2** resulted in removal of 20 – 32 % of biofilm biomass as measured by crystal violet staining and 24 – 73 % reduction in the metabolic activity of cells within the biofilm, using resazurin reduction assays. Cytotoxicity to cultured human keratinocytes was minimal at antimicrobial concentrations but increased with higher concentrations, for **Ir1** but not **Ir2** (**Ir1** $p \leq 0.01$, 5 *Vs* 50 μM). The quantum yield for singlet oxygen ($^1O_2$) emission was measured as 0.16 and 0.30 for **Ir1 and Ir2** respectively. Ground and excited state UV–Vis absorption, steady-state and time-resolved studies together with cyclic voltammetry are also presented. In summary, the potent and rapid antimicrobial activity of these cyclometalated iridium (III) complexes against *S. aureus* and MRSA, which included biofilm eradication, highlight their potential in the management or prevention of device-associated infections or healthcare transmission involving these pathogens.

1. Introduction

Antibiotics have revolutionised modern medicine. Since the introduction of the first antibiotic, penicillin in 1942, global life expectancy has increased and deaths due to infection have decreased [1]. However, the significant health gains in reducing mortality and morbidity are threatened by the rise of antimicrobial resistance (AMR). AMR has now emerged as a chronic public health problem globally, with the forecast

* Corresponding authors.
E-mail addresses: mary.pryce@dcu.ie (M.T. Pryce), dfitzgeraldhughes@rcsi.ie (D. Fitzgerald-Hughes).
[1] Current address: Novus Diagnostics, Dublin City University, Glasnevin Campus, Dublin, D09 NR58.
[2] Joint authors.

https://doi.org/10.1016/j.jphotochem.2024.116218
Received 17 June 2024; Received in revised form 18 October 2024; Accepted 8 December 2024
Available online 12 December 2024

of 10 million deaths per year globally by 2050 [2] as well as an additional economic impact of $1.5 billion to healthcare systems [3]. Infections caused by antibiotic resistant bacteria can lead to longer hospital stays, more severe infections, greater risk of death and an economic burden on healthcare systems [4,5]. The built hospital environment also provides recalcitrant niches in which pathogens can survive for long periods within biofilms. High touch surfaces in particular are reservoirs frequently contaminated with bacteria from human skin, e.g., *Staphylococcus aureus* including methicillin resistant *S. aureus* (MRSA) which can be transmitted onwards to vulnerable patients.

Biofilms are communities or aggregates of heterogeneous microbial cells, coated in a protective matrix of extracellular polymeric substances (EPS) that colonize and infect indwelling medical devices or wounds, as well as surfaces and water systems in the built hospital environment [6]. Biofilms are recalcitrant to antibiotics and liquid disinfectants due to impeded penetration [7,8], and reduced antibiotic susceptibility or high disinfectant tolerance of bacteria in biofilm growth mode, due to altered physiology, slower metabolic activity and high organic loads [9]. Biofilms can persist in chronic infections despite longer courses and higher antibiotic concentrations of antimicrobial therapy. In addition, they can persist in the built healthcare environment despite regular disinfection, which contributes further to the potential for AMR development and risk of patient acquisition.

There is an unmet clinical need for novel antimicrobial agents, with new mechanisms of action capable of killing AMR pathogens while also specifically targeting biofilms. Photodynamic therapy (PDT) is a modality of therapy used for the treatment of cancer and various skin diseases in patients. PDT is also used increasingly in dentistry, in the treatment of oral cancer, bacterial and fungal infections [10]. Antimicrobial photodynamic therapy (aPDT) has much potential for clinical applications that involve AMR and biofilms, such as novel treatment of device-associated infections. Furthermore, photodynamic disinfection can provide highly controlled and targeted disinfection of high-risk healthcare surfaces and equipment, such as those frequently touched by human hands. Briefly, aPDT involves the use of a photosensitizer (PS), which, when irradiated, can generate reactive oxygen species (ROS), including singlet oxygen. Singlet oxygen ($^1O_2$) is a potent antimicrobial agent [11]. It can damage microbial cellular components including proteins, lipids, membranes and nucleic acids [12]. Lipid peroxidation by singlet oxygen leads to membrane leakage and loss of cell integrity [12]. Singlet oxygen can also induce the production of secondary ROS, such as hydrogen peroxide in aqueous environments, which also have antimicrobial properties [13,14].

Recently, transition metal complexes have been extensively assessed as antimicrobial agents [15–19]. Ir(III) complexes have long been investigated as photosensitising agents due to their long-lived triplet excited state and a tolerance to photo-bleaching [20]. Many iridium complexes that have been assessed for antibacterial activity are based on 'half-sandwich' type complexes [21–27]. The kinetically inert cyclometalated iridium (III) species however, are less studied for antimicrobial applications, despite their desirable characteristics [28–31]. In cyclometalated iridium compounds delocalization of the π-electrons over the rings of the chelated ligands increases lipophilicity and penetration of the bacterial cell membranes, thus leading to bacterial growth inhibition. Therefore, cyclometalated Ir(III) complexes have been used for both anticancer and antimicrobial activities and also as photosensitizers in antimicrobial photodynamic therapy [32,33].

Here we show that singlet oxygen generation following irradiation of two novel cyclometalated Ir(III) complexes **Ir1** and **Ir2** (Scheme 1) results in potent antimicrobial activity against *S. aureus* but limited cytotoxicity to human keratinocytes in culture. The anti-biofilm properties of the complexes included significant biofilm-eradication activity including loss of biofilm viability under irradiation. We also report the time-resolved studies of the iridium complexes **Ir1** and **Ir2** using transient absorption and time-resolved emission spectroscopy to investigate the photodynamics of both complexes. The electrochemical properties of the complexes offered insights into the redox chemistry and nature of the frontier molecular orbitals.

2. Experimental section

All chemicals and solvents were supplied by Aldrich Chemicals Co. and anhydrous solvents containing sure/seal were used under a flow of nitrogen. All manipulations were performed with rigorous exclusion of air using standard Schlenk-tube techniques. The starting material [Ir(μ-Cl)(ppy)$_2$]$_2$ (ppy: phenyl pyridine) was prepared according to methods reported in the literature. The NMR spectra were recorded on a Bruker 600 MHz spectrometer and referenced to the deuterated solvent peak as an internal reference. C, H, and N analyses were carried out in a PerkinElmer 2400 CHNS/O analyser. Mass spectroscopy was measured on an Esquire 3000 + with an IonTrap detector interfaced to an Agilent 1100 series HPLC system. All UV–Vis and emission spectra were recorded using a Horiba Duetta Fluorescence and Absorbance spectrometer. Emission and excitation spectra were taken with an absorbance of 0.2 at 375 nm in standard 1 cm quartz fluorescence cuvette. Time-resolved photoluminescence measurements and transient absorption maps were recorded using an Edinburgh Instrument LP980 Transient absorption spectrometer, coupled to a Quantel Q-Smart 450 laser, tuned to the third harmonic. Spectra were obtained with an excitation wavelength of 355 nm with a laser pulse energy of 2 mJ. The samples were prepared to an optical density of 0.2 at 355 nm, in spectroscopic grade solvent (Sigma-Aldrich, purity > 99.9 %). Prior to the measurement, the samples were put under a nitrogen environment by means of three freeze pump-thaw cycles. The optical density of the sample was recorded and compared, before and after the experiment to check for photo-degradation. The results of the experiments were processed using Edinburgh instruments, L900® software.

Electrochemical measurements were performed at room temperature

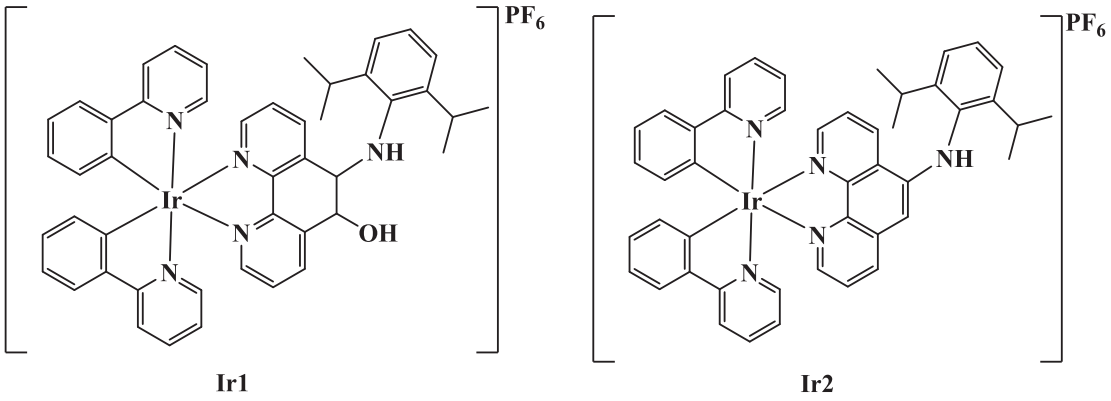

Scheme 1. The structures of the iridium complexes Ir1 and Ir2.

using a CHI 750C Electrochemical Workstation for cyclic voltammetry or a BioLogic VSP potentiostat for differential pulse voltammetry. The electrolytes were 1 mM solutions of the complexes in dry acetonitrile/0.1 M tetrabutylammonium hexafluorophosphate ($TBAPF_6$). A standard 3-electrode cell setup was employed with a glassy carbon disk working electrode and a platinum wire counter electrode. The reference electrode was of the Ag^+ non-aqueous type, comprising of a silver wire immersed in a 0.01 M $AgNO_3$/0.1 M $TBAPF_6$/acetonitrile solution and separated from the rest of the cell by a porous frit. The electrolyte solutions were purged with a stream of dry nitrogen gas for 20 min prior to measurement, and a blanket of nitrogen was maintained above the solution during measurement. The reference electrode was calibrated against ferrocene (a 1 mM solution in 0.1 M $TBAPF_6$/acetonitrile) after each measurement, and all potentials are reported relative to the ferrocenium/ferrocene (Fc^+/Fc) couple.

2.1. Synthesis

2.1.1. Synthesis of ligand 6-((2,6-diisopropylphenyl)amino)-5,6-dihydro-1,10-phenanthrolin-5-ol (L1)

A mixture of 1,10-Phenanthroline 5,6-Epoxide (3.0 g, 15.3 mmol), 2,6-diisopropylaniline (5.7 g, 32.4 mmol), p-Toluene sulfonic acid (0.12 g) in MeOH (70 mL) was brought to reflux temperature for 5 days. Subsequently it was cooled to room temperature, filtered and the solvent removed to obtain an oily residue. This was then washed with hexane (10 mL × 2) and put in vacuo to remove the solvent. Chloroform (100 mL) was added to the flask and filtered. The chloroform was removed, and acetone (25 mL) was added. The flask was placed in the fridge overnight which resulted in precipitation of white solid, which was collected by filtration. Yield: 2.73 g, 47.8 %. ^{1}H NMR (600 MHz, $CDCl_3$, 298 K): δ = 8.71 (dd, 1H), 8.68 (dd, 1H), 7.77 (dd, 1H), 7.38 (dd, 1H), 7.21 (dd, 4.8 Hz, 1H), 7.08 (dd, 1H), 6.97 (s, 3H), 4.98 (d, 1H), 4.30 (d, 1H), 3.95–2.94 (br, 2H), 2.70 (sept, 2H), 1.00 (d, 6H, $CH(CH_3)_2$), 0.89 (d, 6H, $CH(CH_3)$).

2.1.2. Synthesis of Ir(III) complex Ir1

A mixture of $[Ir(\mu\text{-}Cl)(ppy)_2]_2$ (0.4 g, 0.373 mmol), ligand (0.278 g, 0.746 mmol), NH_4PF_6 (0.243 g, 1.49 mmol) in CH_2Cl_2 (30 mL) was brought to reflux temperature for two days. It was subsequently cooled to room temperature and filtered and the solvent removed to obtain an oily residue. The crude product was purified by column chromatography using 1:1:1 (DCM: Ether: Hexanes) mixture. **Ir1** was recrystallised from acetone by the addition of hexane yielding a bright yellow solid which was collected by filtration. Yield: 0.355 g, 46.7 %. ^{1}H NMR (600 MHz, $CDCl_3$, 298 K): δ = 8.42 (d, 1H), 8.12 (d, 1H), 7.88–7.93 (m, 3H), 7.74–7.80 (m, 4H), 7.66–7.69 (m, 3H), 7.42–7.40 (m, 2H), 7.39 – 7.37 (m, 2H), 7.17–7.06 (m, 5H), 6.91–7.04 (m, 2H), 6.37 (d, 1H), 6.32 (dd, 1H), 5.75 (d, 1H), 4.73 (dd, 1H), 3.22 (sept, 2H), 1.25 (d, 6H, CH(CH_3)$_2$), 1.22 (d, 6H, CH(CH_3). ^{13}C NMR ($CDCl_3$): δ = 167.9 (CH_{Ar}), 166.9 (CH_{Ar}), 151.7 (CH_{Ar}), 151.6 (CH_{Ar}), 150.1 (CH_{Ar}), 149.8 (CH_{Ar}), 148.8 (CH_{Ar}), 148.7 (CH_{Ar}), 143.8 (CH_{Ar}), 143.7 (CH_{Ar}), 143.3 (CH_{Ar}), 141.3 (CH_{Ar}), 138.1 (CH_{Ar}), 138.0 (CH_{Ar}), 137.9 (CH_{Ar}), 137.7 (CH_{Ar}), 137.3 (CH_{Ar}), 132.0 (CH_{Ar}), 131.6 (C_{qr}), 130.9 (CH_{Ar}), 130.4 (CH_{Ar}], 128.2 (CH_{Ar}), 128.0 (CH_{Ar}), 124.5 (CH_{Ar}), 124.2 (CH_{Ar}), 123.2 (CH_{Ar}), 122.6 (CH_{Ar}), 122.5 (CH_{Ar}), 119.42 (CH_{Ar}), 119.1 (CH_{Ar}), 74.2 (CH), 63.8(CH), 27.9 (CH(CH_3), 24.1 (CH(CH_3), 24.0 (CH(CH_3). ^{31}P NMR ($CDCl_3$): δ = −144.7 (sept, PF_6). CHN cald: C54.22; H4.25; N6.87, Found: C54.27; H4.23; N6.84. TOF-MS: *m/z* 874.30 (M-PF_6).

2.1.3. Synthesis of the Ir(III) complex Ir2

A mixture of the **Ir1** (0.216 g, 0.212 mmol) and K_2CO_3 (0.180 g, 1.27 mmol) in acetonitrile (20 mL) was heated at 50 °C for 2 days. All solvents were removed and re-dissolved in dichloromethane and filtered over Celite. Concentration of the solution and the addition of hexane led to precipitation of a yellow solid. Yield: 0.185 g, 87.3 %. ^{1}H NMR (600 MHz, $CDCl_3$): δ = 9.32 (d, 1H), 8.28 (d, 1H), 7.87–7.97 (m, 4H), 7.71–7.76 (m, 4H), 7.48–7.49 (m, 1H), 7.40–7.46 (m, 3H), 7.30–7.34 (m, 2H), 6.92–7.11 (m, 7H), 6.38–6.42 (m, 3H), 3.25 (sept, 2H), 1.23 (m, 6H, CH(CH_3)$_2$), 1.09 (m, 6H, CH(CH_3). ^{13}C NMR ($CDCl_3$): δ = 168.2 (CH_{Ar}), 167.7 (CH_{Ar}), 150.9 (CH_{Ar}), 150.3 (CH_{Ar}), 149.9 (CH_{Ar}), 149.0 (CH_{Ar}), 148.3 (CH_{Ar}), 147.7 (CH_{Ar}), 147.4 (CH_{Ar}), 147.2 (CH_{Ar}), 145.1 (CH_{Ar}), 143.7 (CH_{Ar}), 143.4 (CH_{Ar}), 141.4 (CH_{Ar}), 138.0 (CH_{Ar}), 137.9 (CH_{Ar}), 135.0 (CH_{Ar}), 134.0 (CH_{Ar}), 133.3 (CH_{Ar}), 132.9 (CH_{Ar}), 131.9 (CH_{Ar}], 131.7 (CH_{Ar}), 131.0 (CH_{Ar}), 130.6 (CH_{Ar}), 128.4 (CH_{Ar}), 126.4 (CH_{Ar}), 125.9 (CH_{Ar}), 124.8 (CH_{Ar}), 124.6 (CH_{Ar}), 124.4 (CH_{Ar}), 124.2 (CH_{Ar}), 123.5 (CH_{Ar}), 122.9 (CH_{Ar}), 122.7 (CH_{Ar}), 122.5 (CH_{Ar}), 119.6 (CH_{Ar}), 119.3 (CH_{Ar}), 100.9 (CH_{Ar}), 28.3 (CH(CH_3), 24.6 (CH(CH_3), 23.6 (CH(CH_3). ^{31}P NMR ($CDCl_3$): δ = -144.7 (sept, PF_6). CHN cald: C55.19; H4.13; N7.00, Found: C55.16; H4.12; N6.98. TOF-MS: *m/z* 856.29 (M-PF_6).

2.2. Singlet oxygen measurements

The singlet oxygen quantum yields were measured based on the near infrared (NIR) emission band at 1270 nm. Singlet oxygen generation experiments were recorded using an Andor InGaAs detector coupled with a Shamrock 163 Spectrograph. The excitation source was a 385 nm diode laser supplied by Thorlabs. All UV spectra were recorded both before and after singlet oxygen measurements with the sample optical density (OD) below 0.3 absorbance units at the excitation wavelength of excitation. $Ru(bpy)_3$ (Φ_Δ = 0.53) [34], was used as a reference. All samples were investigated in aerated solvent at room temperature. The singlet oxygen quantum yields were calculated using the following formula:

$\Phi_{sample} = \phi_{ref}(Area_{sample}\cdot Abs_{ref})/(Area_{ref}\cdot Abs_{sample})$ where ϕ_{ref} is the singlet oxygen quantum yield of the standard (in the same solvent), $Area_{sample}$ and $Area_{ref}$ are the integrated area between 1200 – 1360 nm of the phosphorescence of singlet oxygen respectively, Abs_{ref} and Abs_{sample} are the absorption of both solutions at 385 nm.

2.3. Bacterial strains and growth conditions

Four bacterial reference strains were used in this study: *E. coli* ATCC 25922, methicillin-sensitive *S. aureus* (MSSA) strains ATCC 25923 and SH1000, methicillin-resistant *S. aureus* (MRSA) strain ATCC 43300. All strains were routinely grown on purity plates of Mueller-Hinton (MH) agar to isolate single colonies.

2.4. Planktonic bactericidal assay

Bacterial suspensions were prepared from isolated colonies to the density of a 0.5 McFarland standard (bioMérieux, Ireland) and were further diluted 1/100 in sterile phosphate buffered saline (PBS), pH 7.4 to a final concentration of approximately 1 × 10^5 colony forming units (CFU)/ml. Stock concentrations of **Ir1** and **Ir2** were prepared in sterile 50 % dimethyl sulfoxide (DMSO) (v/v in PBS) and stored for up to one week at 5 °C, in glass containers, protected from light.

For assays, 180 μL of bacterial suspension (1 × 10^5 CFU/mL) was added to wells of two sterile, 96-well plates (Nunc, Denmark). Ir-complex stock at 10X the assay concentration was added to wells to a final volume of 200 μL. Negative controls contained, either 20 μL of 50 % sterile DMSO or sterile PBS instead of Ir-complex and were included in assays conducted both in the absence of light and when irradiated. Assays of each condition were performed in triplicate and repeated three times. One 96-well plate was exposed for 15 min at room temperature to an LED light source emitting at370 nm (see Fig. S13 in the Supplementary Information (SI) for the emission spectrum of the 370 nm light source) at a distance of 30 mm approximately (Dose = 153 mJ cm^{-2}). The diameter of the beam from the light source at the samples under irradiation was approximately 5 mm. The second 96-well plate was incubated in the dark for 15 min at room temperature. After incubation, samples were pipette mixed to ensure homogeneity and bacterial

viability was assessed using the Miles and Misra method as previously described [35] briefly, serial dilutions of samples were prepared in sterile PBS. Three 20 µL aliquots of each dilution were plated on Mueller Hinton (MH) agar and incubated overnight at 37 °C in a static incubator. Following incubation, colonies were counted, and bactericidal activity for each condition, was determined based on $\log_{10}$ reduction in CFU/mL compared to an untreated negative control.

2.5. Biofilm growth and treatment

Overnight cultures of *S. aureus* were grown in MH broth at 37 °C, 150 rpm and diluted to approximately 1 x 10^6 CFU/mL in MH broth. Aliquots of 200 µL of diluted bacterial culture was added to wells of two sterile 96-well plates (Nunc, Denmark) and incubated statically overnight at 37 °C. Growth media was removed after each 24 h period and replaced with fresh, sterile media. After 72 h, unattached cells were removed by gentle washing with sterile PBS, twice. Excess liquid was removed by drying the surface in a laminar airflow cabinet for 30 min. For testing, 50 % DMSO or PBS (untreated, negative controls) or 100 µL of 50 µM Ir-complex solution, was added to the mature biofilms. The 96-well plate was exposed to an LED light of 370 nm, as described above, for 15 min. After treatment, liquid was removed, and biofilms were gently washed with PBS to remove non-adherent cells and any residual Ir-complex. Biofilms were dried in a laminar airflow cabinet for 30 min.

2.6. Resazurin assay for metabolic activity

Following treatments, biofilm viability was analysed using the non-fluorescent redox dye resazurin (Sigma Aldrich, Ireland) as described previously [36]. Briefly, 200 µl of resazurin solution (88 µM in MH) was added to dried biofilms. The plate was covered with aluminium foil and incubated at 37 °C for 1 h. Fluorescence, which is produced when resazurin is reduced to resorufin by metabolically active cells was measured at 544 nm excitation and 590 nm emission using a Fluorimeter (Victor X3, 2030 Multi-label Reader, Perkin Elmer, Ireland). Experiments were performed in triplicate, three times. Percentage changes in fluorescence intensity compared to the untreated (negative) controls were determined.

2.7. Crystal violet staining for biofilm adherence

Biofilm that remained adherent to wells following treatment with the iridium complex compared to untreated wells was investigated by staining with 0.1 % (w/v) crystal violet (CV) (Sigma Aldrich, Ireland) and incubating at room temperature for 1 h. Biofilms were gently washed with deionised water three times to remove excess stain. Surfaces were air dried for 1 h. CV was solubilised with 100 µL 95 % ethanol and 0.05 % Triton-X-100 (Sigma Aldrich, Ireland) for 30 min. Absorbance was measured at 590 nm in a Victor X3 2030 Multi-label Reader, Perkin Elmer, Ireland). Experiments were performed in triplicate and repeated three times. Reduction in CV-stained biomass (representing loss of adherent biofilm) was represented as percentage change in absorbance intensity relative to controls.

2.8. Cytotoxicity assays

A human keratinocyte cell line (HaCaT) was used. Cells were routinely cultured in Dulbecco's modified Eagle's medium (DMEM) supplemented with 10 % (v/v) fetal bovine serum (FBS) and maintained at 37 °C and 5 % CO_2 atmosphere. Cells were passaged/harvested by detaching from tissue culture flasks using TrypLE TM Express (Gibco) for 5–10 min at 37 °C. HaCaT cells were seeded in 96-well plates at a density of 1 x 10^5 cells/ml in 100 µl culture medium (DMEM with 10 % (v/v) FBS) and incubated at 37 °C, 5 % CO_2 for 48 h for cell attachment. Plates were washed with 100 µl PBS and treated with Ir-complexes as described earlier with a final concentration of either 5 µM or 50 µM for 15 min with and without irradiation (370 nm). Untreated (negative) control wells were incubated with either 5 % DMSO or PBS instead of Ir-complexes. Positive control wells (100 % cell death) were treated with 1 % triton X-100 (v/v in sterile PBS) instead of Ir-complex. Following treatment, wells were washed with 100 µl PBS before adding 100 µl DMEM with 10 % (v/v) FBS. Plates were incubated at 37 °C and 5 % CO_2 for 24 h. To determine metabolic activity, freshly prepared MTT (3-(4,5-dimethylthiazol-2-yl)-2,5-diphenyltetrazolium bromide) (100 µl of 5 mg/ml in culture medium without FBS or supplements) was added to each well, followed by incubation for 4 h at 37 °C with 5 % CO_2. The medium was discarded, and the cells were washed with PBS before adding 100 µl of fixative solution (isopropanol) and incubating at room temperature with shaking for 4 min. Absorbance at 595 nm was measured (Victor X3 2030 Multilabel Reader, Perkin Elmer, Ireland). Cytotoxicity was represented as percentage change of absorbance intensity compared to positive control, which was taken to be 100 % viable.

2.9. Statistical analysis

All statistical analysis was performed using Prism Statistical Software (version 8.3.0, GraphPad, USA). Multiple comparisons among groups was by ordinary one-way ANOVA or comparison of means between two groups was by unpaired *t*-test. *p*-values of ≤0.05 were considered statistically significant and are denoted in results by a star symbol (* $p \leq 0.05$, ** $p \leq 0.01$, *** $p \leq 0.001$, NS = not statistically significant, $p > 0.05$).

3. Results

3.1. Synthesis

The iridium complexes were prepared according to the synthetic scheme displayed in Scheme 2. The cyclometalated iridium(III) chloro-bridged dimer $[Ir(\mu\text{-}Cl)(ppy)_2]_2$ (ppy: phenyl pyridine) was prepared by following the literature [37]. Ligand (L1) was synthesised by heating 1,10-Phenanthroline 5,6-Epoxide and 2,6-diisopropylaniline to reflux temperature in the presence of p-Toluene sulfonic acid in MeOH. The iridium(III) complex Ir1 was synthesized in by the reaction of L1 with the dimer $[Ir(\mu\text{-}Cl)(ppy)_2]_2$ in CH_2Cl_2. The iridium(III) complex Ir2 was synthesised by reaction complex Ir-1 and K_2CO_3 in acetonitrile. Complexes **Ir1** and **Ir2** were characterized by ^1H, ^{13}C, ^{31}P NMR, LC MS, and elemental analysis. The ^1H and ^{13}C, ^{31}P NMR spectra of the free ligands L1 and complexes **Ir1** and **Ir2** were recorded in $CDCl_3$ (Figs. S1–S7, Supporting information) and show all the expected signals. Moreover, the formation of **Ir1** and **Ir2** is clearly evident by the parent peaks in the mass spectra of $(M - PF_6)^+$ centered at m/z = 874.30 and 856.29, respectively (Figs. S8, S9, Supporting information).

3.2. Uv–visible and emission spectroscopy

The UV–visible and emission spectra of **Ir1** and **Ir2** are presented in Fig. 1. The absorption spectra of the compounds are similar in profile to that of $[Ir(ppy)_2(bpy)](PF_6)$ and are described below. Both compounds absorb strongly in the region between 240 nm and 270 nm, arising from ligand centred π–π* transitions, in both the ppy and phenanthroline ligands [38,39]. Like other cationic iridium (III) complexes [40,41], the weak low-energy absorption bands between 310 and 425 nm are assigned to mixed (^{1}CT) transitions resulting from a combination of metal-to-ligand and ligand-to-ligand CT transitions (^{1}MLCT and ^{1}LLCT, respectively), arising from Ir dπ–π_{phen} and π_{ppy}–π^*_{phen} transitions. Above 400 nm, spin forbidden transitions, both ^{3}MLCT and ^{3}LLCT, are seen for both compounds, tailing out to 530 nm in each case. Both compounds are emissive, with a λ_{max} observed at 580 nm for **Ir1** and 605 nm for **Ir2** respectively. It should be noted that presence of the OH in **Ir1** results in a redshift in the emission compared to **Ir2**, due to the electron withdrawing nature of the OH group [39]. Ir**1** displays an emission lifetime

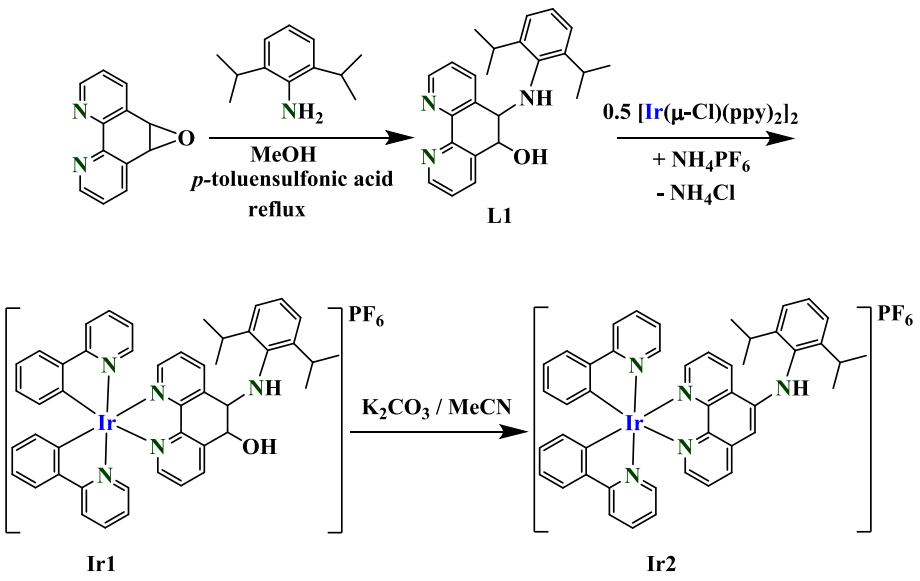

Scheme 2. Synthetic route to ligand (L1), and the Ir(III) complexes **Ir1** and **Ir2**.

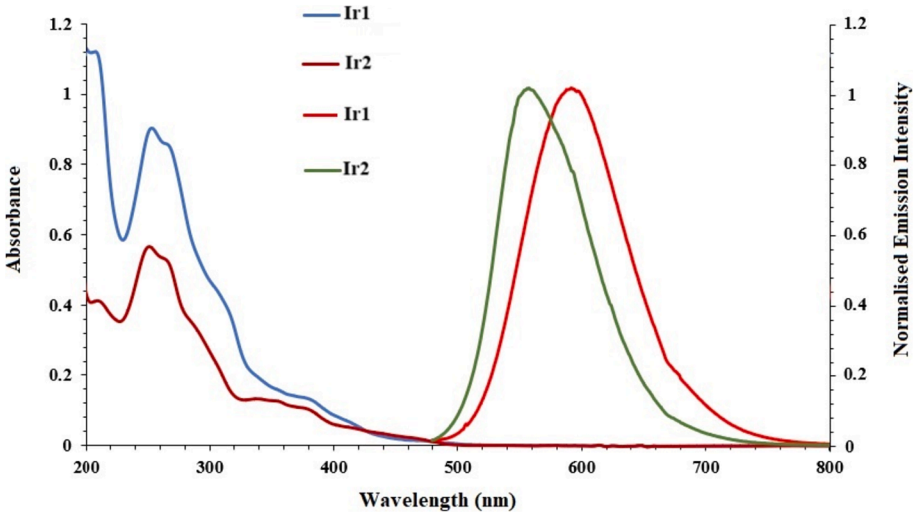

Fig. 1. Normalised absorption and emission spectra (using λ_{exc} 375 nm) for **Ir1** and **Ir2** (0.015 mM) in acetonitrile solution at 298 K.

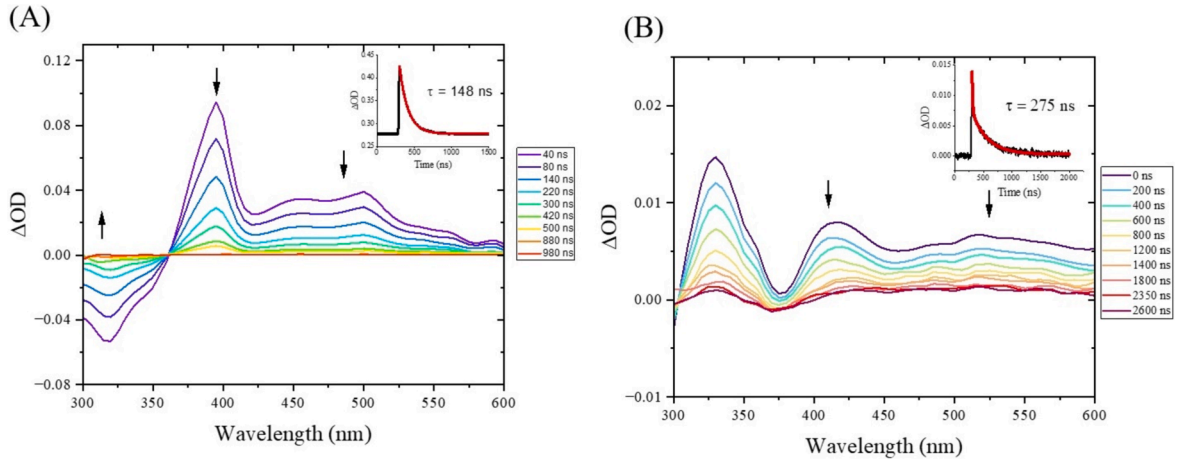

Fig. 2. (A) The transient absorption spectra of **Ir1** in deaerated THF following excitation at 355 nm. The insert shows the kinetic trace recorded at 390 nm. (B) The transient absorption spectra of **Ir2** in deaerated THF following excitation at 355 nm. The insert shows the kinetic trace recorded at 390 nm.

of 148/179 ns in THF/$CHCl_3$. Similarly, for **Ir2**, a lifetime of 277/360 ns was obtained in THF/$CHCl_3$ respectively These lifetimes are assigned to population of mixed ^{3}MLCT/^{3}LLCT excited states.

3.3. Time resolved photophysical measurements

Nanosecond transient absorption spectroscopy, (λ_{ex} = 355 nm) was carried out in two solvents (See Fig. 2, Fig. S10, Table 1). The shape and profile of the transient species observed differs somewhat for both compounds. In the case of **Ir1**, a strong excited state absorption feature is present between 360 nm – 550 nm, which decays on the nanosecond time scale. This excited state species is attributed to a mixed MLCT-LLCT triplet state, localized at the ancillary ligand. This observation is in agreement with the literature [38,42], where lifetimes in the range ca. 180 ns- to ca. 450 ns have been observed by others. In the case of **Ir2** however, there is a considerably more pronounced absorption feature in the range 500 – 600 nm and is tentatively attributed to an increase in ^{3}LLCT character. The lifetimes observed for **Ir2** are longer than **Ir1** in both solvents (for example in THF 148 vs 275 ns). This difference is lifetimes is tentatively assigned to the influence of the –OH unit in **Ir1**. This has previously observed by other researchers, where the presence of electron donating groups leads a modification of the HOMO-LUMO gap [43].

3.4. Singlet oxygen generation

The singlet oxygen quantum yields for both **Ir1** and **Ir2** were measured in air equilibrated acetonitrile against [$Ru(bpy)_3$] by the integration of the $^1O_2$ emission signal at ca. 1270 nm. The quantum yield for $^1O_2$ emission was measured as 0.16 and 0.30 for **Ir1** and **Ir2**, respectively. The singlet oxygen quantum yields for both iridium complexes is less than that of similar complexes in the literature where singlet oxygen quantum yields up to 0.5 have been reported [44].

3.5. Electrochemical properties

Cyclic voltammograms (CVs) of the two complexes are presented in Fig. 3, and the data is summarised in Table 2. In the reduction (negative potential) region, each compound exhibits a substantially reversible redox wave, with formal potentials, E_0^{red}, of −1.72 V and −1.80 V for **Ir1** and **Ir2**, respectively. Electrochemical data has previously been reported for [Ir(III)$(ppy)_2$–1,10-phenanthroline] and various substituted derivatives, and there is a general consensus that this first, one-electron, reversible feature arises due to reduction of the ancillary ligand – i.e: the LUMO sits on the diimine group [39,45]. The appropriateness of this assignment to **Ir2** is underlined by the similarity of the measured E_0 value to others reported in the literature and attributed to phenanthroline-based ligand reduction [46–49]. The cathodic shift of ~ 0.08 V for **Ir2** relative to **Ir1** is consistent with the increase in electron density in the phenanthroline core upon aromatization.

In the positive potential region, compounds based on [Ir(III)$(ppy)_2$–1,10-phenanthroline] often present a one-electron, (quasi-) reversible redox wave that is attributed to the $Ir^{III/IV}$ couple with a significant contribution from the ppy ligands [39,46,50]. It is evident from Fig. 3 that a more complicated scenario prevails for **Ir1** and **Ir2**, where there appears to be a partial superposition of current peaks. Differential pulse voltammetry offers greater resolution in such cases, and

Table 1
A summary of the emission lifetimes for Ir-1 and Ir-2 in THF and $CHCl_3$.

Compound	Solvent	Lifetime
Ir-1	THF	148 ns
Ir-1	$CHCl_3$	179 ns
Ir-2	THF	275 ns
Ir-2	$CHCl_3$	360 ns

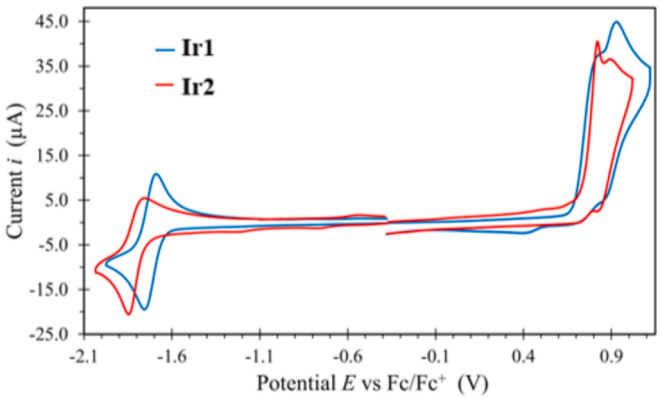

Fig. 3. Cyclic voltammograms recorded from 1 mM solutions of **Ir1** and **Ir2** with 0.1 M $TBAPF_6$ in acetonitrile as background electrolyte. The traces in the reductive and oxidative regions were recorded separately to avoid artefacts. Scan rate was 0.1 $V.s^{-1}$.

Table 2
Summary of the electrochemical properties of Ir1 and Ir2.

	E_0^{ox1} V[a]	E_0^{oxyy} V[b]	E_0^{red} V[b]	HOMO eV[c]	LUMO eV[c]	$\Delta E_{H\text{-}L}$eV
Ir1	0.75	0.89	−1.72	−5.55	−3.08	2.47
Ir2	0.80	0.86	−1.80	−5.60	−3.00	2.60

[a] Derived by the inflection method (i.e. where $\frac{d^2i}{dE^2} = 0$) for an irreversible wave.
[b] Calculated from the average of the anodic and cathodic peak potentials for a (quasi-)reversible wave.
[c] HOMO = $-e(E_0^{ox1}) + (-4.8\ eV)$, LUMO = $-e(E_0^{red}) + (-4.8\ eV)$.

measurements (Fig. S11) suggest the presence of two distinct redox processes in this potential range for each complex. Returning to the CVs, it seems that the initial oxidation event is irreversible for both compounds, while the subsequent process exhibits a degree of reversibility as evidenced by the 'heel' feature (above 0.8 V) on the reverse, negative-direction sweep. In fact, similar voltammetric profiles have been reported previously for related iridium complexes where a substituted phenanthroline ligand contains one or more amine groups [45,48–52]. We therefore propose that the first oxidation of **Ir1** and **Ir2** proceeds at the secondary amine on the ancillary ligand (irreversible), with the typically-expected, mixed metal-ppy oxidation (quasi-reversible) occurring sequentially, at a somewhat higher potential. This suggests that the HOMO for these compounds is predominantly located on the amine fragment of the ancillary ligand and is situated just above the HOMO-1 which is delocalised across the metal centre and the cyclometalating ligands. Elsewhere, DFT calculations have predicted similar molecular orbital sequences for several Ir(III)$(ppy)_2$ based complexes containing amino-substituted 1,10-phenanthroline ancillary ligands [48,53]. The formal potentials for these oxidation reactions are noted in Table 2– in each case E_0 for the $Ir^{III/IV}$-ppy based process (E_0^{ox2}) was calculated as the average of the second anodic peak potential and the cathodic 'heel' potential, while the inflection-point approach [54] was applied to the irreversible first anodic feature (E_0^{ox1}). A cathodic shift of ~ 0.05 V was observed in E_0ox^1 for **Ir1** compared to **Ir2**. This is consistent with the observation that aromatic rings tend to be more electron withdrawing towards substituents relative to aliphatic analogues [55], thereby reducing the electron density at the amine in **Ir2** and making oxidation more difficult. A broad cathodic feature with a maximum at ~ 0.39 V is also obvious in the CV trace of **Ir1**. This is apparently related to a kinetically inhibited reduction of the initial oxidation product (amine-related). Such a response is absent in the case of **Ir2**, pointing to a difference between the two complexes regarding the

reactivity and/or stability of the first oxidised species. The energies of the frontier orbitals on the vacuum scale were derived from the first oxidation and reduction potentials and are tabulated along with the HOMO-LUMO energy gaps, $\Delta E_{H\text{-}L}$, in Table 2. The increase in $\Delta E_{H\text{-}L}$ for **Ir2** compared to **Ir1** is consistent with the spectroscopic blue-shifts noted in section 3.2 for the former, relative to the latter.

3.6. Photostability of the compounds

The photostability of the **Ir1** and **Ir2** was evaluated by irradiating at 370 nm, in acetonitrile. No detectable changes were observed in the UV–Vis spectrum after 2 h of irradiation, confirming the stability of **Ir1** and **Ir2** under these conditions (Fig. S12).

3.7. Antimicrobial properties of iridium complexes

Exposure of *S. aureus* and *E. coli* to light (no complexes) at 370 nm, for 15 min, resulted in negligible reduction in cell numbers of < 0.24 log CFU/ml indicated no loss of viability due to the irradiation conditions alone. When incubated with *S. aureus* (ATCC 25923) for 15 min, **Ir1** and **Ir2** at 5 μM exhibited 4.5 and 4.6 $\log_{10}$ reduction in CFU/mL respectively after exposure to light at 370 nm, which was at the upper limit of the assay. However, in the absence of light bacterial inactivation was less than 1 $\log_{10}$ reduction in CFU/mL for both iridium complexes, indicating a low level of dark toxicity. **Ir1** and **Ir2** poorly inactivated the Gram-negative bacterium *E. coli* (ATCC 25922) at 5 μM under both dark and light conditions (Fig. 4). Against *S. aureus*, the antibacterial effects of both Ir-complexes were concentration dependent (Fig. 5). Decreasing concentrations of **Ir1** or **Ir2** from 5 μM to 0.1 μM correlated with a decrease in antibacterial activity from 4.5 to 1.1 $\log_{10}$ CFU/mL (**Ir1**) and from 4.6 to 1.7 $\log_{10}$ CFU/mL (**Ir2**). The iridium complexes also showed anti-biofilm properties against mature 3-day old *S. aureus* (MSSA and MRSA) biofilms. For MSSA (SH1000) biofilms, 15 min incubation of the iridium complexes (at 370 nm) reduced adherent biofilm biomass as shown by CV staining. Reduced cell viability within the biofilms was also apparent, from resazurin staining for metabolic activity (Fig. 6A). Light activation, and treatment with the iridium complexes, led to loss of 40 % (**Ir1**) and 65 % (**Ir2**) of MSSA biofilm biomass and inactivated 46 % and 48 % of bacteria within the MSSA biofilms respectively. In comparison, for the MRSA strain (ATCC 44330) **Ir1** and **Ir2** were less effective in reducing biofilm biomass (20 % and 32 %, for **Ir1** and **Ir2** respectively) under the same treatment conditions. However, greater

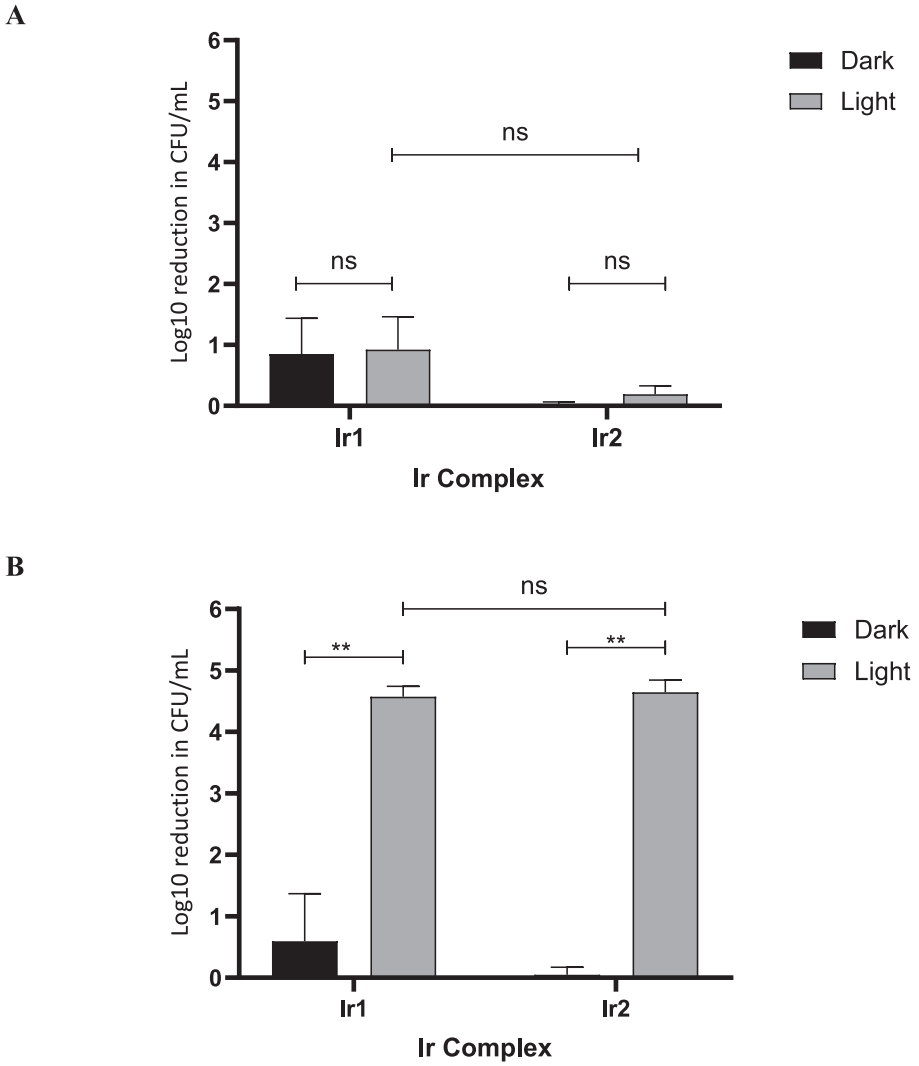

Fig. 4. Bactericidal effect of Ir-complexes against planktonic *E. coli* (A) and *S. aureus* (B) in dark *Vs* light conditions. Ir-complexes (5 μM) were incubated with bacteria of initial concentration 1×10^5 CFU/mL. Samples were incubated either in the dark (black bars) or under a light source of 370 nm (grey bars) for 15 min. Resulting bacterial viability was determined through CFU assays and results are displayed as mean ± SD $\log_{10}$ reduction in CFU/ml with respect to DMSO control for three separate assays performed in triplicate. Statistical analysis of means for light *Vs* dark conditions and for **Ir1** *Vs* **Ir2** are shown, where ** = $p \leq 0.01$, ns = not statistically significant.

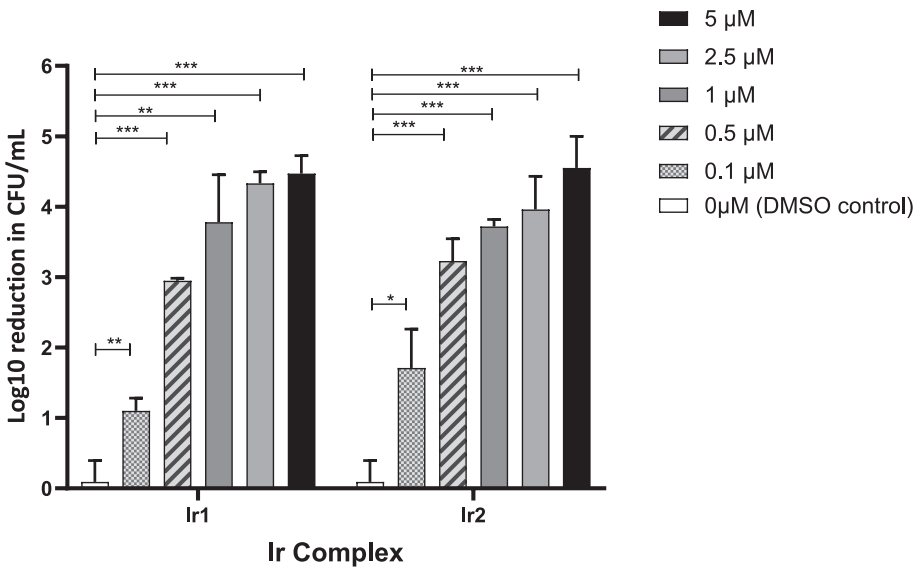

Fig. 5. Concentration dependence of Ir-complex photoactivated bactericidal activity. Ir-complexes of varying concentrations (5 μM – 0.1 μM) or DMSO (control) were incubated with *S. aureus* 25,923 at 1 × 10^5 CFU/ml. Bacterial viability was determined following irradiation at 370 nm, (153 mJ cm^{-2}) for 15 min using CFU assays. Activity in dark conditions was subtracted. Results are displayed as mean ± SD log_{10} reduction in CFU/mL for three separate assays performed in triplicate. Statistical analysis of means for each concentration compared to the DMSO control using unpaired *t*-test are shown where *** = $p \leq 0.001$, ** = $p \leq 0.01$, * = $p \leq 0.05$.

inactivation of MRSA within biofilms resulted for both iridium complexes (73 % and 59 % respectively) (Fig. 6B).

3.8. Cytotoxicity investigation

At the concentration effective in killing planktonic cells, cytotoxicity towards keratinocytes was negligible for **Ir1** with 95 % and 94 % of cells remaining viable in dark and light conditions respectively. A similar cytotoxicity profile was found for **Ir2** under both light and dark conditions, with cellular viability ranging from 75-77 % (Fig. 7B). Overall, no statistically significant differences between cell viability under light and dark conditions for either complex was found. However, at 50 μM, the concentration used to investigate anti-biofilm effects against *S. aureus,* **Ir1** was cytotoxic towards human keratinocytes with only 20 % and 29 % of HaCaT cells remaining viable following treatment. This concentration dependent cytotoxicity was not apparent for **Ir2** (in dark conditions and light conditions respectively (Fig. 7)).

4. Discussion

Without effective antibiotics, and effective disinfection for items such as medical instruments, catheters, surgical tools, and high-contact surfaces adjacent to the patient care areas. the gains made in modern medicine, to enhance quality of life, will be lost due to unacceptably high risk of infection. Novel antimicrobial agents, that have mechanisms completely different to those of current antibiotics and targeted innovative physical disinfection approaches are critical in this regard [56]. Many infections (e.g., surgical site infection) involve bacteria in biofilms and in addition, biofilms can develop on in-dwelling medical devices (e.g., catheters, pacemakers, artificial joints) or healthcare surfaces and water systems, making these sites prone to unresolving infection or reservoirs for AMR transmission [57,58]. Therefore, novel antimicrobial agents should also be effective against bacteria biofilms. Where biofilms exist, greater antibiotic and biocide concentrations are required to penetrate the protective carbohydrate and protein rich structures and to inactivate cells within, which often have altered metabolic properties compared to planktonic cells [59,60]. Novel antimicrobial agents should also have low cytotoxic activity for use as a medicinal treatment.

The iridium complexes investigated here, demonstrate some of the required properties of potential future antimicrobials, with perhaps greater potential in surface disinfection applications. They had differing antibacterial activity against the two bacteria tested in this study, *E. coli* and *S. aureus*. Most bacteria can be grouped into two classes, Gram-negative and Gram-positive. Gram-negative bacteria, such as *E. coli*, contain an outer cell membrane while Gram-positive bacteria, such as *S. aureus*, have no outer membrane and are instead coated in a thick layer of peptidoglycan [61]. Due to these structural differences, Gram-negative and Gram-positive bacteria can differ in their permeability and sensitivity to biocides and antibiotics [62,63]. This has also been observed in aPDT. For example, Maisch *et al.*, [64] assessed the use of a singlet oxygen producing PS against *S. aureus* and *E. coli* and found strong antibacterial activity against *S. aureus* and little activity against *E. coli*. This corresponded to the uptake of the PS by the respective bacterial strain. The differing antibacterial activity of the iridium complexes could be due in part to the differing permeability of the bacterial strains. However, further studies are required to confirm this.

Both iridium complexes showed strong antibacterial activity against planktonic *S. aureus*, completely inactivating bacteria after irradiation for 15 min. No bacterial inactivation was seen in dark samples not exposed to light and light alone caused negligible cell killing. This pattern correlates to singlet oxygen production by both complexes. This study was assessed using 10^5 CFU/mL bacterial concentrations, which would be considered a moderate to heavy bacterial load [65]. Previous aPDT studies have shown similar inactivation of planktonic bacteria. *Lu et al.* [66], showed a 7.5 log_{10} reduction in *S. aureus* viability after a 4-minute treatment with oxidising, thymol-based PS agents. With visible light, the use of novel PS agents could be of use as, not only a stand-alone treatment, but also as an adjunct to current, empiric treatment. A recent study by *Liu et al.* [67], assessed the use of a well-studied singlet oxygen producing PS agent, toluidine blue against multi-drug resistant *S. aureus*. This study showed that although some bacterial inactivation was achieved through PS treatment alone (1.7 log_{10}) or with the antibiotic gentamicin alone (0.7 log_{10}), greater bacterial inactivation could be achieved when both treatments were used in combination. Our study has shown strong antibacterial activity against *S. aureus* (>4.5 log_{10}), albeit requiring irradiation at 370 nm. While **Ir1** showed little toxicity to human skin cells *in vitro*, under irradiation, this wavelength may be poorly tolerated in clinical use, except for very short periods.

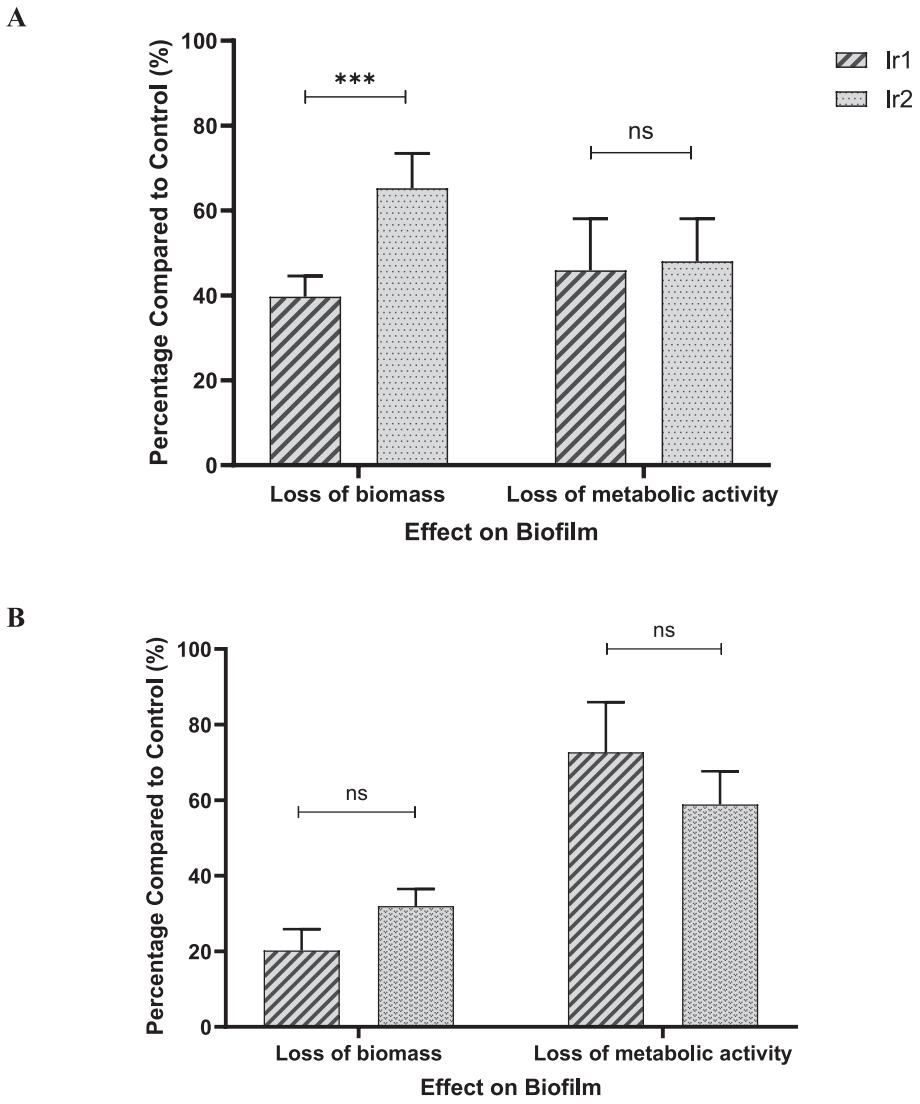

Fig. 6. Antibiofilm effects of Ir-complexes against MSSA (a) and MRSA (b) biofilms. *S. aureus* biofilms were grown for 72-hours on MH. Biofilms were then treated with Ir-complexes (50 μM) and exposed to light (370 nm, 153 mJ cm^{-2}) for 15 min. Loss of adherent biofilm was measured using CV assays and bacterial metabolic activity in biofilms was measured using resazurin reduction assays. Results are expressed as percentage of untreated control biofilms (mean ± SD, 6 replicates from two assays). Statistical analysis of means by unpaired *t*-test for **Ir1** *Vs* **Ir2** are shown, *** = $p \leq 0.001$, ns = not statistically significant.

Nonetheless, where specific, rapid *S. aureus*/MRSA targeting, are important, such as surface disinfection of high hand-touch or multiple user equipment adjacent to patients, the Ir complexes show potential application.

When developing novel antimicrobial agents, it is important to inactivate not only planktonic bacteria, but also bacterial biofilms. Bacteria in biofilms can confer a much higher resistance to antimicrobial treatment and greater tolerance to liquid disinfectants compared to planktonic cells [68,69]. Our study has shown antibiofilm effects against mature, 3-day biofilms resulting in some inactivation of biofilm-associated bacteria, as well as loss of adherent biomass. For effective biofilm eradication, it is important to not only inactivate microorganisms within the biofilm, but also to limit biofilm adherence [70]. Several studies have shown reactive oxygen species producing PS, curcumin, to inactivate bacteria within *S. aureus* biofilms [71–73] and removal some of the biofilm biomass [71]. Oxidising agents, such as those used in aPDT, are often found to have greater effect against microbial biofilm than traditional biocides. This is thought to be due, in part, to the damage caused to the DNA, proteins and lipids that make up the protective extracellular polysaccharide substances (EPS) coating of biofilms [60,74]. Akhtar et al., [72] demonstrated a significant reduction in EPS after treatment with a curcumin PS. The inactivation and removal of biofilms shown in this study could be due to the singlet oxygen produced during PS treatment (0.16 – 0.30), which can inactivate bacteria as well as disrupt the biofilm structure.

Novel antimicrobial agents should be investigated for cytotoxicity as well as antimicrobial activity. Effective antimicrobial agents should show inactivation of microorganisms at concentrations that do not induce extensive toxicity against human cells. A potential application of PS agents could be as a topical treatment for wound infection and in this study, we examined the cytotoxicity of Ir-complexes against human epithelial cells. We showed that cytotoxicity was not irradiation dependant. Pellissari *et al.*, [75] also – showed similar cytotoxicity of epithelial cells after treatment with and without irradiation of a singlet oxygen producing PS agent. In this study, we have displayed differing cytotoxicity for each iridium complex. A 15-minute incubation with low concentrations of **Ir1** (5 μM) resulted in high levels of cellular viability. However, at high concentrations of **Ir1** (50 μM), resulted in some inactivation of epithelial cells. Previous studies have also shown concentration dependant cytotoxicity of aPDT [76,77]. At low complex concentrations (5 μM), both complexes showed little adversary viability against epithelial cells even with light activation, while providing strong

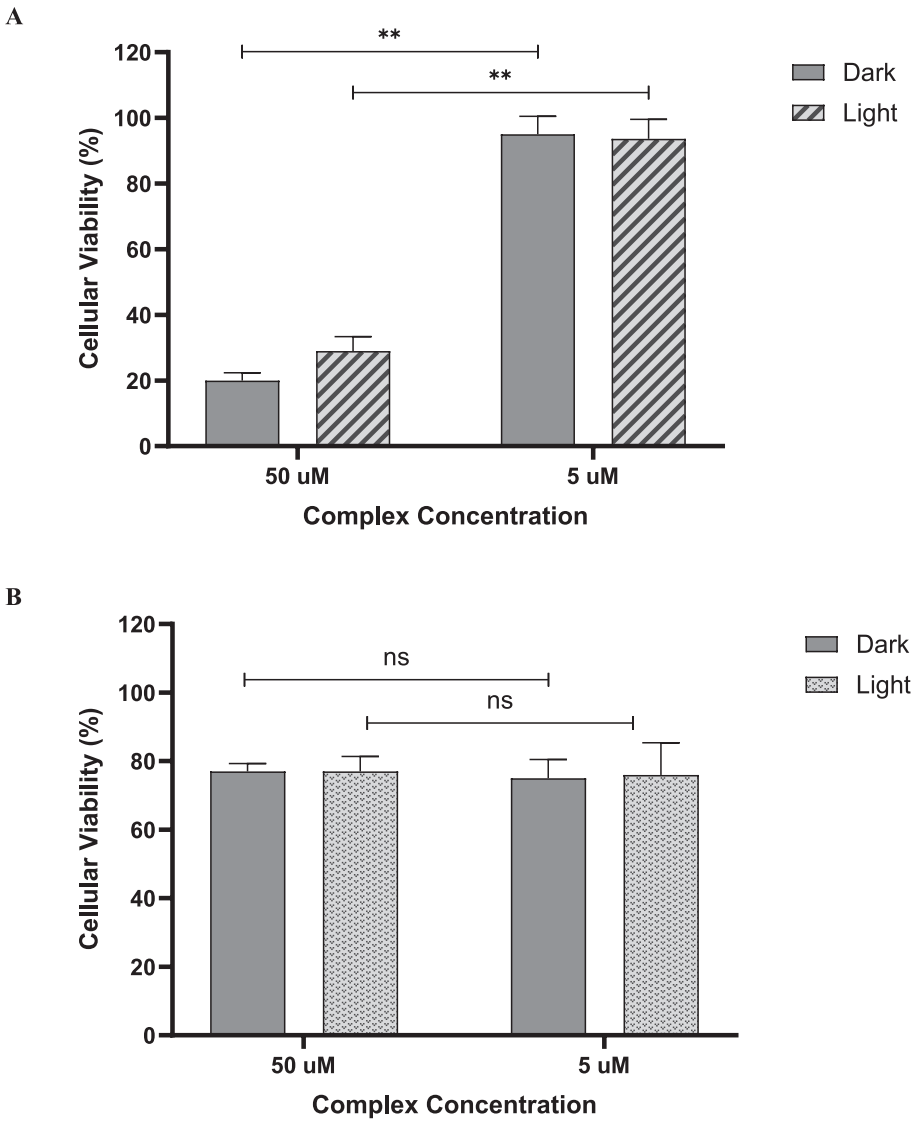

Fig. 7. *In-vitro* cytotoxicity of Ir-complexes (a) **Ir1** and (b) **Ir2** against human keratinocytes. Human keratinocytes were grown to maturity and incubated with Ir-complexes of either 50 μM or 5 μM in the dark, or under a light source of 370 nm, 153 mJ $cm^{-}2$ for 15 min. Viability of cells was measured using MTT assays and results are shown as percentage that remained viable compared to an untreated negative control. Mean ± SD, for three assays in triplicate are presented. Statistical analysis of mean for 5 μM *Vs* 50 μM by unpaired *t*-test are shown, ** = $p \leq 0.01$, ns = not significant.

antibacterial activity. Further work should be completed examining efficient therapeutic dosages, limiting harm to human cells and maximising antimicrobial action. Human skin poorly tolerates light below the visible spectrum and further structural modifications should be rationalised towards higher light wavelengths for medical applications, or other applications that do not require skin exposure, such as pathogen targeted disinfectant application should be explored.

Busto et al., also showed microbial inactivation with iridium(III) PS against Gram-positive bacteria (*Enterococcus faecium* and MRSA) with no antimicrobial activity seen against Gram-negative bacteria (*Acinetobacter baumanii* and *Pseudomonas aeruginosa*). This study also showed that the antibacterial activity in *S. aureus* did not result in membrane damage, perhaps suggesting that the differing activity against Gram-positive and −negative bacteria may be due to differing cellular envelopes The Ir(III) compounds $[Ir(C\hat{}N)_2(N\hat{}N)](PF_6)$, (where N^N = 1-methyl-1H-pyrazole [3́,4́:5,6]pyrazino [2,3-f] [1,10]phenanthroline and C^N = 2-phenylpyridine), demonstrated bactericidal activity when assessed against Gram-negative bacteria *Klebsiella pneumoniae* (white led light) with > 99.9 % inactivation [78]. The iridium complexes show significant potential in aPDT, as evidenced by their activity shown in Figs. 4 to 7.

The compounds **Ir1** and **Ir2** display photophysical properties analogous to their less modified counterparts. Both complexes populate the triplet states, with lifetimes ranging from 148 to 360 ns, which is sufficiently long lived to generate singlet oxygen. Modification of the chelated phenanthroline, by removal of an –OH group with H, leads to differences in the photophysical properties of **Ir2** compared to **Ir1**. Such changes influence the HOMO/LUMO gap, which in turn lead to a change in the population of the MTCT/ LLCT states. This alteration can be further exploited to design more effective PDT agents. Regarding the frontier orbital separation energies, consistency was observed between the spectroscopic and electrochemical data, with the comparative redshift in emission wavelength for **Ir1** also reflected in a smaller electrochemical HOMO-LUMO gap for this complex relative to **Ir2**. The voltammetry measurements also revealed closely separated, upper occupied, ground-state energy levels for these complexes. In each case, this was interpreted in terms of an orbital, related to the amine site on the ancillary ligand, lying marginally above the delocalised metal C^N ligand orbital that generally presents as the HOMO in similar reported compounds.

This ability to tune their electronic properties enables iridium complexes to effectively produce reactive oxygen species that can target and destroy bacterial cells, offering a promising alternative to traditional antimicrobial treatments. Key advantages of using these iridium complexes in aPDT are the avoidance of conventional antibiotic targets, for which antimicrobial resistance mechanisms exist and the ability to precisely control the treatment area through targeted light activation. The design of these complexes, particularly the choice of ligand **L1** plays a crucial role in enhancing the solubility, and overall therapeutic effectiveness.

5. Conclusions

This study has shown the potential use of two light-activated, singlet oxygen producing iridium complexes, **Ir1** and **Ir2** as novel antimicrobial agents. Both emission and transient absorption studies indicates population of triplet excited states for both complexes. The quantum yield for $^1O_2$ emission, a potent antimicrobial agent was 0.16 and 0.30 for **Ir1** and **Ir2**, respectively [79]. From our studies it is clear that modification of the bipyridyl ligand influences both the photophysical and electrochemical properties. The straightforward elimination reaction that converted **Ir1** to **Ir2** had the effect of raising the LUMO level (more negative reduction potential). Antibacterial activity was observed after 15-minute treatment with light irradiation. However, antibacterial effectiveness differed between bacterial strains, *E. coli* and *S. aureus*, possibly due to cellular structure. Both iridium complexes were shown to partially inactivate and remove mature *S. aureus* biofilms. Little cytotoxicity was observed against human epithelial cells when incubated with low concentrations of the iridium complexes, however, this could be concentration dependent. The penetration depth of 370 nm light is sufficient for topical applications, but human skin can only tolerate this wavelength for short periods. Therefore, further structural modifications of **Ir1**/**Ir2** should be directed towards their activation in the visible spectrum to avoid damage to healthy skin with repeat doses. In conclusion, our study demonstrates that cyclometalated iridium (III) complexes activated by 370 nm exhibit potent antimicrobial properties against *S. aureus* and MRSA, including biofilm disruption. While irradiation at 370 nm poses challenges for direct skin applications, these complexes show promise as light-activated agents for surface disinfection, such as in medical settings, industrial applications, and on medical devices.

CRediT authorship contribution statement

Muireann Fallon: Writing – original draft, Methodology, Formal analysis, Data curation. **Ralte Lalrempuia:** Visualization, Validation, Methodology, Investigation, Funding acquisition, Formal analysis, Data curation, Conceptualization. **Leila Tabrizi:** Visualization, Methodology, Investigation, Formal analysis, Data curation, Conceptualization. **Michael P. Brandon:** Methodology, Investigation, Formal analysis, Data curation. **Ross McGarry:** Visualization, Validation, Investigation, Formal analysis, Data curation. **Aoibhín Cullen:** Methodology, Investigation, Formal analysis, Data curation. **Francisco J. Fernández-Alvarez:** Methodology, Investigation, Formal analysis, Data curation. **Mary T. Pryce:** Writing – review & editing, Supervision, Resources, Project administration, Methodology, Funding acquisition, Conceptualization. **Deirdre Fitzgerald-Hughes:** Writing – review & editing, Supervision, Resources, Project administration, Methodology, Funding acquisition, Conceptualization.

Declaration of competing interest

The authors declare that they have no known competing financial interests or personal relationships that could have appeared to influence the work reported in this paper.

Acknowledgements

Funding for this project is gratefully acknowledged from Research Ireland (RI) (19/FFP/6882, 19/FFP/6956), the European Commission, through a Marie Sklodowska – Curie Fellowship to RL (No. 799778) and the EU Commission Recovery and Resilience Facility under the Research Ireland, Healthy Environment for All, Challenge Grant Number 22/NCF/HE/11252.

Appendix A. Supplementary data

Supplementary data to this article can be found online at https://doi.org/10.1016/j.jphotochem.2024.116218.

Data availability

Data will be made available on request.

References

[1] K.I. Mohr, History of Antibiotics Research, Curr. Top. Microbiol. Immunol. 398 (2016) 237–272. https://pubmed.ncbi.nlm.nih.gov/27738915.
[2] K.W.K. Tang, B.C. Millar, J.E. Moore, Br. J. Biomed. Sci. 80 (2023) 11387, https://doi.org/10.3389/bjbs.2023.11387. PMID: 37448857; PMCID: PMC10336207.
[3] D.M. Sievert, P. Ricks, J.R. Edwards, A. Schneider, J. Patel, A. Srinivasan, A. Kallen, B. Limbago, S. Fridkin, Infect. Control Hosp. Epidemiol. 34 (1) (2013) 1–14, https://doi.org/10.1086/668770.
[4] M. Stillo, S. Scoffone, S. Passi, C.M. Zotti, Epidemiol. Prev. 38 (2014) 93–97.
[5] S. Manoukian, S. Stewart, S. Dancer, N. Graves, H. Mason, A. McFarland, C. Robertson, J. Reilly, J. Hosp. Infect. 100 (2) (2018) 222–235, https://doi.org/10.1016/j.jhin.2018.06.003.
[6] H.C. Flemming, J. Wingender, U. Szewzyk, P. Steinberg, S.A. Rice, S. Kjelleberg, Nat. Rev. Microbiol. 14 (2016) 563–575.
[7] R. Singh, S. Sahore, P. Kaur, A. Rani, P. Ray, Pathog. Dis. 74 (6) (2016) ftw056, https://doi.org/10.1093/femspd/ftw056.
[8] A. Singh, S. Padmesh, M. Dwivedi, I. Kostova, Infect. Drug Resist. 15 (2022) 503–532. http://www.ncbi.nlm.nih.gov/pubmed/35210792.
[9] O. Ciofu, E. Rojo-Molinero, M. D. Macià, A. Oliver, APMIS. 125(4) (2017) 304–31http://doi.wiley.com/10.1111/apm.12673.
[10] K. Konopka, T. Goslinski, Photodynamic therapy in dentistry, J. Dent. Res. 86 (8) (2007) 694–707.
[11] G. Zampini, O. Planas, F. Marmottini, O. Gulías, M. Agut, S. Nonell, L. Latterini, RSC Adv. 7(24) (2017) 14422–9. https://pubs.rsc.org/en/content/articlehtml/2017/ra/c7ra00784a.
[12] J. Glaeser, A.M. Nuss, B.A. Berghoff, G. Klug, Adv. Microb. Physiol. 58 (2011) 141–173. https://pubmed.ncbi.nlm.nih.gov/21722793/.
[13] J.A. Imlay, Adv. Microb. Physiol. 46 (2002) 111–153.
[14] J.A. Imlay, Nat. Rev. Microbiol. 11 (2013) 443–454.
[15] M. Patra, G. Gasser, N. Metzler-Nolte, Dalton Trans. 41 (2012) 6350–6358.
[16] M. Patra, M. Wenzel, P. Prochnow, V. Pierroz, G. Gasser, J.E. Bandow, N. Metzler-Nolte, Chem. Sci. 6 (2015) 214–224.
[17] D.K. Weber, M.-A. Sani, M.T. Downton, F. Separovic, F.R. Keene, J.G. Collins, J. Am. Chem. Soc. 138 (2016) 15267–15277.
[18] P. Chellan, V.M. Avery, S. Duffy, J.A. Triccas, G. Nagalingam, C. Tam, L.W. Cheng, J. Liu, K.M. Land, G.J. Clarkson, I. Romero-Canelón, P.J. Sadler, Chem. – Eur. J. 24 (2018) 10078–10090.
[19] K.L. Smitten, S.D. Fairbanks, C.C. Robertson, J. Bernardino de la Serna, S.J. Foster, J.A. Thomas, Chem. Sci. 11 (2020) 70–79.
[20] M. He, F. Chen, D. Shao, P. Weis, Z. Wei, W. Sun, Biomaterials 275 (2021) 120915.
[21] F. Chen, J. Moat, D. McFeely, G. Clarkson, I.J. Hands-Portman, J.P. Furner-Pardoe, F. Harrison, C.G. Dowson, P.J. Sadler, J. Med. Chem. 61 (2018) 7330–7344.
[22] B.F. Hohlfeld, B. Gitter, C.J. Kingsbury, K.J. Flanagan, D. Steen, G.D. Wieland, N. Kulak, M.O. Senge, A. Wiehe, Chem. – Eur. J. 27 (2021) 6440–6459.
[23] B.P.R. Aradhyula, M. Kalidasan, K. Gangele, D.K. Deb, S.L. Shepherd, R.M. Phillips, K.M. Poluri, M.R. Kollipara, Chem. Select 2 (2017) 2065–2076.
[24] A.B.P. Rao, N.R. Palepu, D.K. Deb, A. Uma, T. Chiranjeevi, B. Sarkar, W. Kaminsky, K.M. Rao, Inorg. Chim. Acta 443 (2016) 126–135.
[25] L. Shadap, N. Agarwal, V. Chetry, K.M. Poluri, W. Kaminsky, M.R. Kollipara, J. Organomet. Chem. 937 (2021) 121731.
[26] N. Baartzes, A. Jordaan, D.F. Warner, J. Combrinck, D. Taylor, K. Chibale, G. S. Smith, Eur. J. Med. Chem. 206 (2020) 112694.
[27] A.M. Mansour, K. Radacki, Dalton Trans. 49 (2020) 4491–4501.
[28] M. Pandrala, F. Li, M. Feterl, Y. Mulyana, J.M. Warner, L. Wallace, F.R. Keene, J. g,, Dalton Trans. 42 (2013) 4686–4694.
[29] N. Jain, P. Alam, I.R. Laskar, J. Panwar, RSC Adv. 5 (2015) (1988) 61983–61986.
[30] E. Sauvageot, M. Elie, S. Gaillard, R. Daniellou, P. Fechter, I.J. Schalk, V. Gasser, J.-L. Renaud, G.L.A. Mislin, Metallomics 9 (2017) 1820–1827.
[31] Q.-Y. Yi, W.-Y. Zhang, M. He, F. Du, X.-Z. Wang, Y.-J. Wang, Y.-Y. Gu, L. Bai, Y.-J. Liu, Jbic,, J. Biol. Inorg. Chem. 24 (2019) 151–169.

[32] L. Lu, L.-J. Liu, W. Chao, H.-J. Zhong, M. Wang, X.-P. Chen, J.-J. Lu, R. Li, D.-L. Ma, C.-H. Leung, Sci. Rep. 5 (2015) 14544.
[33] N. Busto, G. Vigueras, N. Cutillas, B. García, J. Ruiz, Dalton Trans. 51 (2022) 9653–9663.
[34] A.A. Abdel-Shafi, P.D. Beer, R.J. Mortimer, F. Wilkinson, Chem. A Eur. J. 104 (2) (2000) 192–202.
[35] A.A. Miles, S.S. Misra, J.O. Irwin, The estimation of the bactericidal power of the blood, J. Hyg. (Lond) 38 (6) (1938) 732–749.
[36] S. Hogan, M. Zapotoczna, N.T. Stevens, H. Humphreys, J.P. O'Gara, E. O'Neill, J. Hosp. Infect. 96 (2017) 177–182.
[37] S. Sprouse, K.A. King, P.J. Spellane, R.J. Watts, J. Am. Chem. Soc. 106 (1984) 6647–6653.
[38] S. Ilic, D.R. Cairnie, C.M. Bridgewater, A.J. Morris, J. Photochem. Photobiol. 8 (2021) 100084, https://doi.org/10.1016/j.jpap.2021.100084.
[39] Y. Kataoka, K. Okuno, N. Yano, H. Ueda, T. Kawamoto, M. Handa, J. Photochem. Photobiol. A Chem. 358 (2018) 345–355, https://doi.org/10.1016/j.jphotochem.2017.09.009.
[40] L. Flamigni, A. Barbieri, C. Sabatini, B. Ventura, F. Barigelletti, Photochemistry and Photophysics of Coordination Compounds: Iridium, Top. Curr. Chem. 281 (2007) 143–203.
[41] S. Ladouceur, E. Zysman-Colman, Eur. J. Inorg. Chem. (2013) 2985–3007.
[42] P. Wang, S. Guo, H.J. Wang, et al., Nat. Commun. 10 (2019) 3155, https://doi.org/10.1038/s41467-019-11099-8.
[43] A.F. Henwooda, E. Zysman-Colman, Chem. Commun. 53 (2017) 807–826.
[44] V.L. Whittle, J.A. Gareth Williams, Inorg. Chem. 47 (15) (2008) 6596–6607, https://doi.org/10.1021/ic701788d.
[45] C. Dragonetti, L. Falciola, P. Mussini, S. Righetto, D. Roberto, R. Ugo, A. Valore, F. De Angelis, S. Fantacci, A. Sgamellotti, M. Ramon, M. Muccini, Inorg. Chem. 46 (21) (2007) 8533–8547.
[46] R.V. Kiran, C.F. Hogan, B.D. James, D.J.D. Wilson, Eur. J. Inorg. Chem. 2011 (2011) 4816–4825.
[47] N.M. Shavaleev, R. Scopelliti, M. Grätzel, M.K. Nazeeruddin, A. Pertegás, C. Roldán-Carmona, D. Tordera, H.J. Bolink, J. Mater. Chem. C 1 (2013) 2241–2248.
[48] H. Tang, Y. Li, Q. Chen, B. Chen, Q. Qiao, W. Yang, H. Wu, Y. Cao, Dyes Pigm. 100 (2014) 79–86.
[49] J. Dong, Y. Dinga, Y. Zhou, Dalton Trans. 51 (2022) 15031–15039.
[50] K.P.S. Zanoni, B.K. Kariyazaki, A. Ito, M. Kyle Brennaman, T.J. Meyer, N. Y. Murakami Iha, Inorg. Chem. 53 (8) (2014) 4089–4099.
[51] P.-K. Lee, W. Ho-Tin Law, H.-W. Liu, K. Kam-Wing Lo, Inorg. Chem. 50 (17) (2011) 8570–8579.
[52] K.J. Castor, K.L. Metera, U.M. Tefashe, C.J. Serpell, J. Mauzeroll, H.F. Sleiman, Inorg. Chem. 54 (14) (2015) 6958–6967.
[53] W. Zhang, F. Zhang, Y.-L. Wang, B. Song, R. Zhang, J. Yuan, Inorg. Chem. 56 (3) (2017) 1309–1318.
[54] E.M. Espinoza, J.A. Clark, J. Soliman, J.B. Derr, M. Morales, V.I. Vullev, J. Electrochem. Soc. 166 (2019) H3175.
[55] G.S. Nolan, L.J. Saethre, M.R. Siggel, T.D. Thomas, L. Ungier, J. Am. Chem. Soc. 107 (23) (1985) 6463–6467.
[56] World Health Organization. Antimicrobial resistance surveillance in Europe. 2022.
[57] M. Magana, C. Sereti, A. Ioannidis, C.A. Mitchell, A.R. Ball, E. Magiorkinis, et al., Clin. Microbiol. Rev. 31 (3) (2018) e00084–e116, https://doi.org/10.1128/CMR.00084-16.
[58] K. Rahim, S. Saleha, X. Zhu, L. Huo, A. Basit, O. L. Franco, Microb Ecol. 73(3) (2017) 710–721. https://pubmed.ncbi.nlm.nih.gov/27742997/.
[59] J.B. Mandell, S. Orr, J. Koch, B. Nourie, D. Ma, D.D. Bonar, N. Shah, K.L. Urish, J. Orthop. Res. 37 (7) (2019) 1604–1609.
[60] K. Tote, T. Horemans, D. Vanden Berghe, L. Maes, P. Cos, Appl. Env. Microbiol. 76 (10) (2010) 3135–3142.
[61] M. Rohde, Microbiol Spectr. 7 (2019) 3, https://doi.org/10.1128/microbiolspec.
[62] P.J. Lillie, G. Johnson, M. Ivan, G.D. Barlow, P.J. Moss, J. Hosp. Infect. 103 (2) (2019) 128–133.
[63] A.D. Russell, Am. J. Infect. Control 29 (2001) 259–261, https://doi.org/10.1067/mic.2001.115671.
[64] T. Maisch, J. Baier, B. Franz, M. Maier, M. Landthaler, R.M. Szeimies, et al., PNAS 104 (17) (2007) 7223–7228, https://doi.org/10.1073/pnas.0611328104.
[65] T. E. Serena, K. Harrell, L. Serena, R. A. Yaakov, J. Wound Care. 28(6) (2019) 346–357. https://pubmed.ncbi.nlm.nih.gov/31166857/.
[66] M. Lu, Y. Li, M.X. Wu, Commun. Biol. 4 (2021) 1, https://doi.org/10.1038/s42003-021-01956-y.
[67] S. Liu, B. Mai, M. Jia, D. Lin, J. Zhang, Q. Liu, P. Wang, Photodiagn. Photodyn. Ther. 30 (2020) 101703. https://pubmed.ncbi.nlm.nih.gov/32151763/.
[68] J.A. Otter, K. Vickery, J.T. Walker, E. deLancey Pulcini, P. Stoodley, S. D. Goldenberg, J.A.G. Salkeld, J. Chewins, S. Yezli, J.D. Edgeworth, J. Hosp. Infect. 89 (1) (2015) 16–27.
[69] P. Gilbert, A.J. McBain, Am. J. Infect. Control 29 (4) (2001) 252–255, https://doi.org/10.1067/mic.2001.115673. PMID: 11486267.
[70] K. Schilcher, A.R. Horswill, Microbiol. Mol. Biol. Rev. 84 (3) (2020) e00026–e119, https://doi.org/10.1128/MMBR.00026-19.
[71] C.G. de S. Teixeira, P. V. Sanitá, A.P. D. Ribeiro, L. M. Dias, J. H. Jorge, A. C. Pavarina, Photodiagnosis Photodyn Ther. 30 (2020) 101760.
[72] F. Akhtar, A.U. Khan, L. Misba, K. Akhtar, A. Ali, Eur. J. Pharm. Biopharm. 160 (2021) 65–76.
[73] S. Torabi, K. Joharchi, K.A.M. Kalhori, M. Sohrabi, R. Fekrazad, Photodiagn. Photodyn. Ther. 33 (2021) 102092. https://pubmed.ncbi.nlm.nih.gov/33212266/.
[74] C. Y. Leung, Y. C. Chan, L. P. Samaranayake, C. J. Seneviratne, J. Hosp. Infect. 81 (2) (2012) 79–86. http://www.sciencedirect.com/science/article/pii/S0195670111004786.
[75] C. V. G. Pellissari, A. C. Pavarina, V. S. Bagnato, E. G. D. O. Mima, C. E. Vergani, J. H. Jorge. Photochem Photobiol Sci. 15 (5) (2016) 682–90. https://pubmed.ncbi.nlm.nih.gov/27110908/.
[76] M. Grinholc, J. Nakonieczna, G. Fila, A. Taraszkiewicz, A. Kawiak, G. Szewczyk, T. Sarna, L. Lilge, K.P. Bielawski, Appl. Microbiol. Biotechnol. 99 (9) (2015) 4031–4043, https://doi.org/10.1007/s00253-015-6539-8.
[77] J.A. Pereira, C.R. Polaquini, V.R. dos Santos, K.S. Caiaffa, R.L. Rabelo, R dos S. Theodoro, L. Helena Theodoro, L. Octavio Regasini, C. Duque, Photodiagn. Photodyn. Ther. 36 (2021) 102534, https://doi.org/10.1016/j.pdpdt.2021.102534.
[78] M. Valenzuela-Valderrama, V. Bustamante, N. Carrasco, I.A. González, P. Dreyse, C. Erick Palavecino, Photodiagn. Photodyn. Ther. 30 (2020) 101662.
[79] S. Noimark, E. Salvadori, R. Gó Mez-Bombarelli, A.J. Macrobert, I.P. Parkin, C.W. M. Kay, PCCP 18 (2016) 28101–28109, https://doi.org/10.1039/C6CP02529C.